PROTEINS
STRUCTURE ■ FUNCTION ■ BIOINFORMATICS

STRUCTURE NOTE

Crystal structure of *Saccharomyces cerevisiae* glutamine synthetase Gln1 suggests a nanotube-like supramolecular assembly

Yong-Xing He,[1] Long Gui,[1] Yin-Zi Liu,[1] Yang Du,[1] Yeyun Zhou,[1] Ping Li,[2]* and Cong-Zhao Zhou[1]*

[1] Hefei National Laboratory for Physical Sciences at Microscale and School of Life Sciences, University of Science and Technology of China, Hefei, Anhui 230026, People's Republic of China

[2] School of Life Sciences and Technology, Tongji University, Shanghai 200092, People's Republic of China

Key words: glutamine synthetase; *Saccharomyces cerevisiae*; crystal structure; supramolecular assembly; structural comparison.

INTRODUCTION

Glutamine synthetase (GS, *EC 6.3.1.2*) is an enzyme that catalyzes the condensation of glutamate and ammonium to form glutamine, with concomitant hydrolysis of ATP.[1] There are three different classes of GS enzymes, referred to as GSI, GSII, and GSIII. GSI enzymes are specific to prokaryotes and form oligomers of 12 identical subunits.[2] The activity of GSI enzyme is regulated by the adenylation of a tyrosine residue.[3] GSII enzymes are found in eukaryotes and some bacteria (Rhizobiaceae, Frankiaceae, and Streptomycetaceae families, which also have GSI). They form decamers of identical subunits.[4] In mammals, GSII enzymes eliminate free ammonia and convert the excitotoxic glutamate into glutamine, which is not neurotoxic.[5] In plants, there are two or more isoenzymes of GSII, which are targets of some herbicides because of their roles in ammonia assimilation. GSIII enzymes were first found in *Bacteroides fragilis* and identified afterward in a few more anaerobic bacteria and cyanobacteria.[6–8] They are hexamers of identical subunits which are much larger (about 700 residues) than that of GSI (450–470 residues) or GSII (350–420 residues) enzymes.[9]

Over the course of two decades, GSI enzymes have been biophysically and structurally characterized.[1–3,10,11] However, little was known about the catalytic mechanism and quaternary structure of the GSII enzymes until the recent publication of GSII structures from maize, human, and canine.[4,12] Structural analyses indicated that GSII and GSI enzymes share a similar catalytic mechanism, implying a common ancestor of these two classes of GS. Moreover, the crystal structures revealed that GSII has the decamer structure consisting of two stacking pentameric rings, instead of the formerly claimed octamer structure inferred from the electronic microscopy studies or sedimentation experiments.[1,13] Because of the relatively fewer crystallographic studies on GSII enzymes, it is necessary to elucidate GSII structures of other species to complete our understandings on GSII enzymes from the structural and biochemical perspective.

In this article, we report the crystal structure of Gln1, a GSII enzyme from *Saccharomyces cerevisiae* that shares high sequence homology with maize GS and human GSII (~55% sequence identity), at the resolution of 2.95 Å.

Grant sponsor: Chinese National Natural Science Foundation; Grant numbers: 20576002, 30470366; Grant sponsor: Ministry of Science and Technology of China; Grant numbers: 2006CB910202, 2006CB806501.

*Correspondence to: Cong-Zhao Zhou, Hefei National Laboratory for Physical Sciences at Microscale and School of Life Sciences, University of Science and Technology of China, Hefei, Anhui 230026, People's Republic of China. E-mail: zcz@ustc.edu.cn or Ping Li, School of Life Sciences and Technology, Tongji University, Shanghai 200092, People's Republic of China. E-mail: liping01@tongji.edu.cn

Received 5 January 2009; Revised 22 January 2009; Accepted 25 January 2009
Published online 10 February 2009 in Wiley InterScience (www.interscience.wiley.com). DOI: 10.1002/prot.22403

Comparative structure analysis suggests that citrate binding could induce structural fluctuation of the segment Leu293-Ala300, which may serve the role of guarding the glutamate entrance to the active sites. Moreover, a novel pentamer–pentamer interface was revealed, implying a nanotube-like supramolecular assembly for Gln1, although the biological significance is still an open question.

METHODS

Construction, expression, and purification of Gln1

The coding sequence of a truncated version of Gln1 (residues 19–370) was cloned into a pET28a-derived vector. This construct adds a hexahistidine (6×His) tag to the N-terminus of the recombinant protein, which was overexpressed in *E. coli* Rosetta(DE3) (Novagen, Madison, WI) strain using 2×YT culture medium (5 g of NaCl, 16 g of bactotrypton, and 10 g of yeast extract per liter). The cells were grown at 37°C up to an $A_{600\ nm}$ of 0.6. Expression of recombinant Gln1 was induced at exponential phase with 0.2 m*M* isopropyl-β-D-thiogalactoside (IPTG) and cell growth continued for another 20 h at 16°C before harvesting. Cells were collected by centrifugation at 4000*g* for 20 min and resuspended in lysis buffer (20 m*M* Tris-Cl, pH 8.0, 200 m*M* NaCl). After 3 min of sonication and centrifugation at 12,000*g* for 25 min, the supernatant containing the soluble target protein was collected and loaded to a Ni-NTA column (GE Healthcare) equilibrated with binding buffer (20 m*M* Tris-Cl, pH 7.0, 200 m*M* NaCl). The target protein was eluted with 250 m*M* imidazole buffer and further loaded onto a Superdex 200 column (Amersham Biosciences) equilibrated with 20 m*M* Tris-Cl, pH 8.0, 200 m*M* NaCl. Fractions containing the target protein were combined and concentrated to 40 mg/mL. The purity of protein was estimated on SDS-PAGE and the protein sample was stored at −80°C.

Crystallization, data collection, and processing

The crystals of Gln1 were grown at 289 K using the hanging drop vapor-diffusion techniques, with the initial condition by mixing 1 μL of the 20 mg/mL protein sample with equal volume of mother liquor (0.2*M* sodium acetate, 0.1*M* sodium citrate, pH 5.5, 8% polyethylene glycol 4000). Typically, crystals appeared in 1 or 2 days and reached to the maximum size in 1 week. The crystals initially did not diffract beyond 5 Å and showed severe anisotropic diffraction pattern. The diffraction resolution and quality was improved by dehydrating the crystals using the method described by Abergel.[14] Several crystals were soaked in a droplet consisting of 9 μL reservoir liquor and 1 μL glycerol. The droplet was left evaporating in the air. At various times, the crystal was flash-frozen and mounted. The diffraction image was recorded at 100 K in a liquid nitrogen stream using a Rigaku MM007 X-ray generator (λ = 1.5418 E) with a MarRearch 345 image-plate detector (USTC, Hefei, China). One crystal soaked for ~1 h diffracted to 2.95 Å and was chosen for the data collection. Data were processed with MOSFLM 7.0.4[15] and scaled with SCALA.[16]

Structure solution and refinement

The crystal structure of Gln1 was determined by the molecular replacement method with MOLREP[17] using the coordinates of a pentamer of human GS in complex with ADP and phosphate (PDB code 2OJW) as the search model. Four pentamers were located in the asymmetric unit. The initial model was refined by using the maximum likelihood method implemented in REFMAC5[18] as part of CCP4i[19] program suite and rebuilt interactively by using the σ_A-weighted electron density maps with coefficients 2Fo-Fc and Fo-Fc in the program COOT.[20] Two percent of the reflections (3299 reflections) was set side to calculate the R-free factor. During the later stage, the restrained positional and B-factor refinement was performed using the program phenix.refine,[21] and tight NCS restraints over the 20 subunits were applied during the refinement. Twenty citrate molecules were located in the final model. Refinement converged to an R-factor of 22.5% and R-free of 25.8% at the resolution of 2.95 Å. The final models were evaluated with the programs MOLPROBITY[22] and PROCHECK.[23] The final coordinates and structure factors were deposited in the Protein Data Bank under the accession code of 3FKY. The data collection and structure refinement statistics were listed in Table I. The buried surface area was calculated with AREAIMOL as part of the CCP4i program suite, and all structure figures were prepared with the program PyMOL.[24]

RESULTS AND DISCUSSION

Overall structure and active site

Initial attempts to crystallize the full length Gln1 were unsuccessful. Because the multiple sequence alignment of GSII enzymes indicates that the N-terminal 18 residues are not highly conserved [Fig. 1(A)], we constructed a truncated version of Gln1 missing the N-terminal residues 1–18 and determined its crystal structure at the resolution of 2.95 Å. The asymmetric unit contains 20 subunits, which are assembled into four pentamers stacking onto one another. Even though the electron density map reveals most features of side chains, few regions where the map is not well resolved exist: N-terminal His-tag, Asp19-Gln20, Asp71-Ser72, Leu293-Ala300 and C-terminal Arg367-Ser370. The final refinement and validation

Table I
Crystal Parameters, Data Collection, and Structure Refinement

	Gln1ΔN18
Data processing	
Space group	P1
Unit cell parameters a, b, c (Å)	128.65, 129.94, 135.61
α, β, γ (°)	93.46, 104.61, 104.01
Resolution range (Å)	65.23–2.95 (3.11–2.95)[a]
Unique reflections	163,752 (23,325)
Completeness (%)	95.1 (92.9)
$\langle I/\sigma(I)\rangle$	7.9 (2.1)
R_{merge}[b] (%)	10.6 (40.7)
Redundancy	2.1
Refinement statistics	
Resolution range (Å)	65.21–2.95
R-factor[c]/R-free[d] (%)	22.5/25.8
Number of protein atoms	53,481
Number of water atoms	0
RMSD[e] bond length (Å)	0.010
RMSD bond angles (°)	1.240
Average of B factors (Å^2)	47.51
Ramachandran plot[f]	
Most favored (%)	94.01
Additional allowed (%)	4.63
Outliers (%)	1.36
PDB entry	3FKY

[a]The values in parentheses refer to statistics in the highest bin.
[b]$R_{merge} = \sum_{hkl}\sum_i|I_i(hkl) - \langle I(hkl)\rangle|/\sum_{hkl}\sum_i I_i(hkl)$, where $I_i(hkl)$ is the intensity of an observation and $\langle I(hkl)\rangle$ is the mean value for its unique reflection; summations are over all reflections.
[c]R-factor $= \sum_h|Fo(h) - Fc(h)|/\sum_h Fo(h)$, where Fo and Fc are the observed and calculated structure-factor amplitudes, respectively.
[d]R-free was calculated with 2% of the data excluded from the refinement.
[e]Root-mean square deviation from ideal values.
[f]Categories were defined by Molprobity.

statistics are acceptable considering the resolution limit (Table I).

The subunit of Gln1 comprises an N-terminal β-grasp domain consisting of a five-strand antiparallel β-sheet and a C-terminal catalytic domain [Fig. 1(B)]. The β-grasp domain from each subunit interacts with the catalytic domain from the neighboring subunit, leading to the assembly of a pentameric ring. Within each pentameric ring, there exist five active sites, located at the interface between each pair of neighboring subunits. The truncated N-terminal residues Met1-Leu18 correspond to a short α-helix termed the meander region in maize and human GSII.[4,12] Although this meander region was proposed to play roles in stabilizing the pentamer,[12] here inferred from our structure, it is at least not essential for the quaternary structure of yeast Gln1.

To investigate the conformational changes of GSII upon substrate binding, we compared the Gln1 structure to human GS in complex with Mn^{2+}, ADP, and the inhibitor MSO-P (HsGS/MnADP/MSO-P, PDB code 2Q8C). Obvious conformational changes were observed at the C-terminal tail composed of residues Gly354-Glu366 and the two disordered regions of residues His70-Ile74 and Arg292-Ser301, respectively [Fig. 1(C)]. The nonconserved C-terminal tail of Gln1 comprises of a short 3_{10} helix preceded by a loop, which seems not to be involved in either catalysis or stabilizing the quaternary structure. The conformation of residues His70-Ile74 is more similar to apo-GSII from canine, consisting with the previous proposal that GSII active sites without ADP binding adopt an open conformation.[12] The missing electron density of residues Arg292-Ser300 implies the high flexibility of this segment, the counterpart of which in HsGS/MnADP/MSO-P is an ordered loop involved in binding the inhibitor MSO-P. It is worth noting that this loop forms steric clashes with the citrate molecule bound in Gln1, suggesting the conformational fluctuation of this segment is mainly due to the citrate binding. Inferred from the corresponding loop of GSI (termed Glu327 flap in GSI),[1] this segment in Gln1 may serve the role of guarding the glutamate entrance to the active site.

The citrate molecule is bound by five residues, Glu193, Gln198, Gly246, His250, and Arg292, in a mode quite similar to that of GSI from *Mycobacterium tuberculosis*.[27] Indeed, citrate was reported to inhibit the activity of GSII in the fungus *Aspergillus niger*, which leads to the citrate accumulation referred to as citrate fermentation.[28] However, it was unclear whether the inhibitory effect is due to the metal ion chelating effects or competitive binding of citrate molecules. Here, the structure of Gln1 suggests a possible inhibitory mechanism of the competitive binding of citrate.

Oligomeric structure

Previously, the crystal structures of maize and mammalian GS indicated the decamer structure for the eukaryotic GSII. As shown in Figure 2(A), the four stacking pentamers in one asymmetric unit are designated as I, II, III, and IV. Pentamers I, II and III, IV form the conserved face-to-face decamers with five twofold axes perpendicular to a fivefold axis. The inter-ring interface buried up to ~1900 Å^2, which constitutes ~3% of the accessible surface area of a single pentamer. In one pentamer, the five loops consisting of residues Met139-Ala153 are involved in the inter-ring contacts and form reciprocal interactions with their twofold symmetry-related mates of the other pentamer. Most interactions are hydrophobic except for 10 hydrogen bonds linking the main-chain oxygen and nitrogen atoms from the five pairs of twofold symmetry-related Tyr151 residues. As reported in human and canine GSII, the active sites in one pentamer are shifted by ~30° relative to those of the other pentamer, which is nearly one half of the fivefold rotation component [Fig. 2(B)]. The whole decamer structure of Gln1 can be well superimposed onto either the human or maize GS decamer, implying a conserved decamer architecture of GSII family.

In addition, the structure of Gln1 revealed a novel back-to-back pentameric ring association formed between pentamers II and III. The buried area for such an inter-

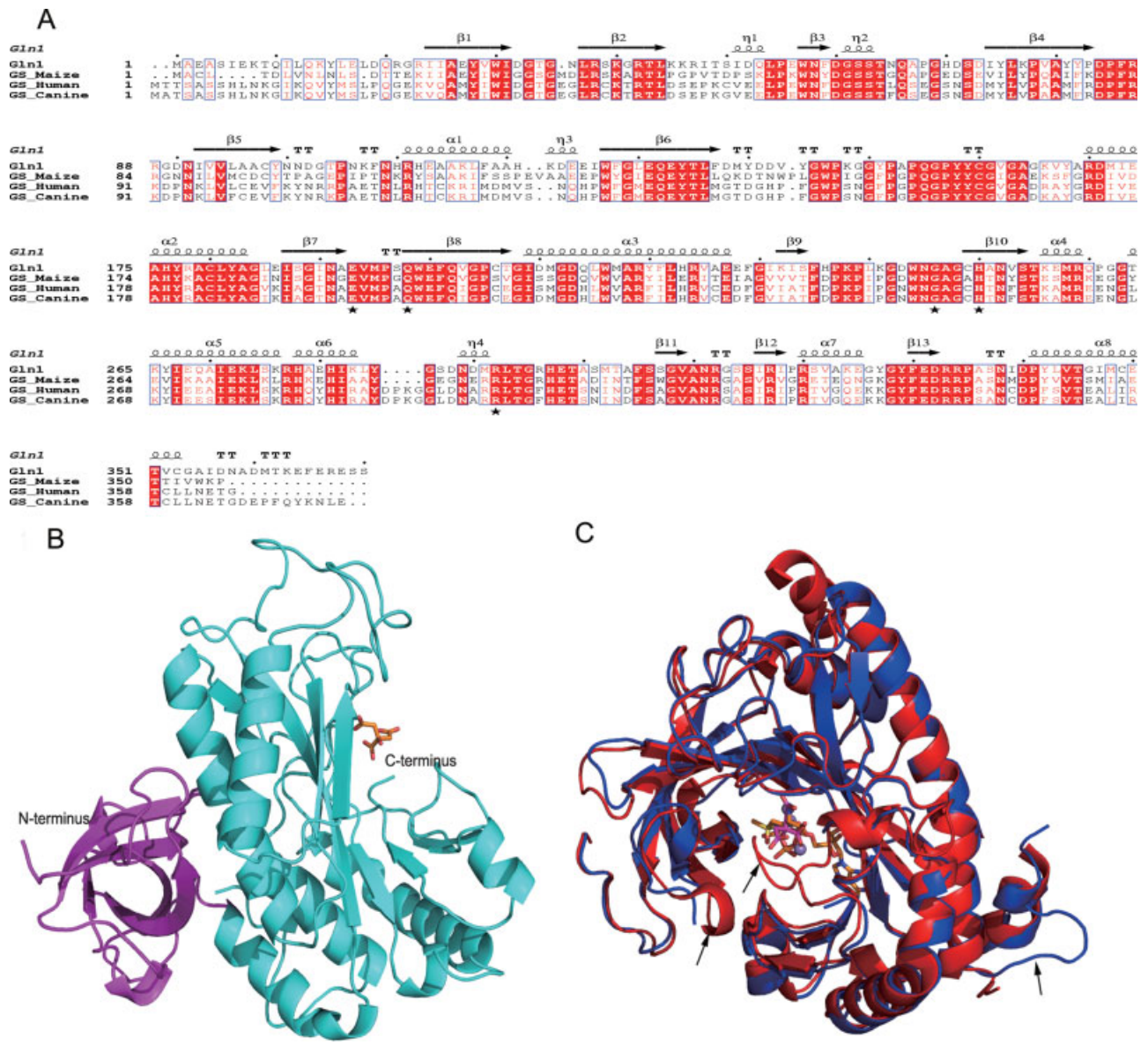

Figure 1

(**A**) Multialignment of GSII enzymes. The alignment was performed using MultAlin and ESPript.[25,26] The secondary structural elements are identified from the structure of Gln1 and displayed at the top of the alignment. The α-helices, η-helices, β-sheets, and strict β-turns are denoted as α, η, β, and TT, correspondingly. The residues involved in citrate binding were marked by black stars. (**B**) Cartoon representation of the Gln1 monomer. The N-terminal β-grasp domain was colored in purple and the C-terminal catalytic domain was colored in green. The bound citrate ion was shown in sticks. (**C**) Superposition of Gln1 (blue) and human GSII in complex with Mn^{2+}, ADP, and the inhibitor MSO-P (red). The regions undergoing large conformational changes were indicated with black arrows. Two neighboring subunits in the pentameric ring were used for the superposition. Only the catalytic domain from one subunit and the neighboring β-grasp domain from the other were shown in cartoon representation. The citrate was shown in pink sticks, ADP and MSO-P in golden sticks, and manganese in gray spheres.

face is ∼1700 Å^2, comparable to the typical face-to-face interface described earlier. This novel interface mainly involves loops consisting of residues Gly22-Arg23 and Lys45-Asp52 in the β-grasp domains. The active sites in one pentamer are shifted by ∼10° relative to those of the other [Fig. 2(C)]. Combining the two types of pentamer–pentamer interfaces together, the pentameric rings of Gln1 could be assembled into a water-filled nanotube with the cylinder diameter of ∼120 Å.

GSI from *E. coli* has been reported to be self-assembled into nanotubes in a divalent metal ion-dependent manner.[29,30] It was suggested that the self-assembled GSI may represent a useful "scaffold." Although at present we do not have biochemical evidence to support the exis-

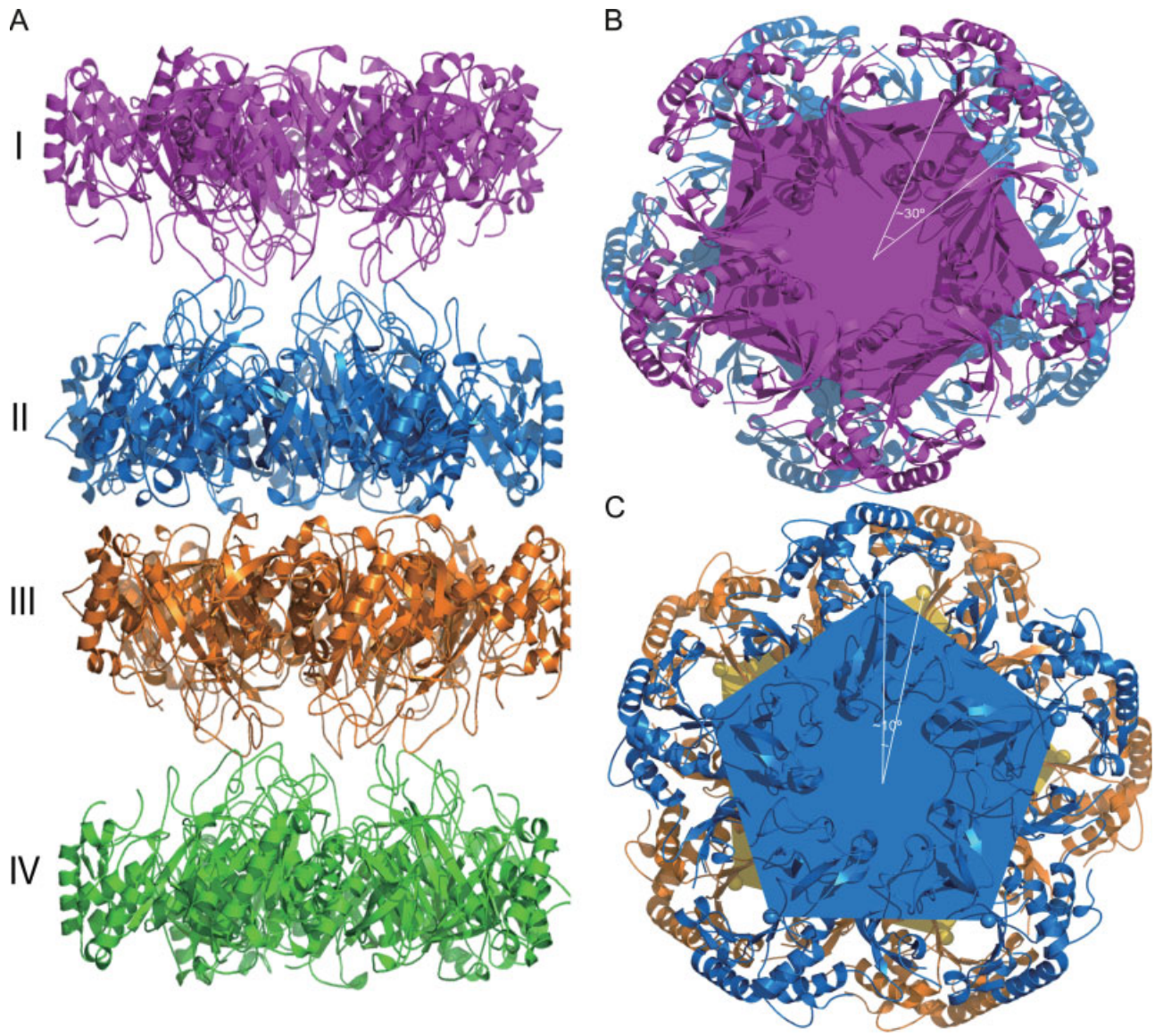

Figure 2

Oligomeric structure of Gln1. (**A**) Cartoon representation of four stacking pentameric rings in one asymmetry unit, designated as pentamer I, II, III, and IV. (**B**) Gln1 decamer composed of pentamer I and pentamer II at the top view. (**C**) The novel back-to-back pentameric ring association involving pentamer II and pentamer III at the top view. For B and C, the pentagons were drawn using the active sites (positions of His250) as vertices in each pentamer.

tence of Gln1 nanotube-like oligomers in solution, we speculate that Gln1 may have the potential to be self-assembled into nanotubes for the following reasons. First, the buried surface area of the novel pentamer–pentamer interface is approximately the same as that of the reported typical inter-ring interface, which was thought sufficiently plausible.[4] Second, the novel pentamer–pentamer interface is related by the noncrystallographic symmetry operator, which means that the formation of this interface is not simply a necessary consequence of crystallization. Finally, a fraction of GSII enzymes from the plant *Phaseolus vulgaris* has been reported to exist as oligomers of higher molecular weight.[13] Further biochemical and biophysical studies are undergoing to confirm the biological significance of this nanotube-like supramolecular assembly for yeast Gln1.

REFERENCES

1. Eisenberg D, Gill HS, Pfluegl GM, Rotstein SH. Structure-function relationships of glutamine synthetases. Biochim Biophys Acta 2000;1477:122–145.

2. Yamashita MM, Almassy RJ, Janson CA, Cascio D, Eisenberg D. Refined atomic model of glutamine synthetase at 3.5 A resolution. J Biol Chem 1989;264:17681–17690.
3. Liaw SH, Pan C, Eisenberg D. Feedback inhibition of fully unadenylylated glutamine synthetase from *Salmonella typhimurium* by glycine, alanine, and serine. Proc Natl Acad Sci USA 1993;90:4996–5000.
4. Unno H, Uchida T, Sugawara H, Kurisu G, Sugiyama T, Yamaya T, Sakakibara H, Hase T, Kusunoki M. Atomic structure of plant glutamine synthetase: a key enzyme for plant productivity. J Biol Chem 2006;281:29287–29296.
5. Derouiche A, Frotscher M. Astroglial processes around identified glutamatergic synapses contain glutamine synthetase: evidence for transmitter degradation. Brain Res 1991;552:346–350.
6. Hill RT, Parker JR, Goodman HJ, Jones DT, Woods DR. Molecular analysis of a novel glutamine synthetase of the anaerobe *Bacteroides fragilis*. J Gen Microbiol 1989;135:3271–3279.
7. Crespo JL, Garcia-Dominguez M, Florencio FJ. Nitrogen control of the glnN gene that codes for GS type III, the only glutamine synthetase in the cyanobacterium *Pseudanabaena* sp. PCC 6903. Mol Microbiol 1998;30:1101–1112.
8. Wen ZT, Peng L, Morrison M. The glutamine synthetase of *Prevotella bryantii* B(1)4 is a family III enzyme (GlnN) and glutamine supports growth of mutants lacking glutamate dehydrogenase activity. FEMS Microbiol Lett 2003;229:15–21.
9. van Rooyen JM, Abratt VR, Sewell BT. Three-dimensional structure of a type III glutamine synthetase by single-particle reconstruction. J Mol Biol 2006;361:796–810.
10. Gill HS, Eisenberg D. The crystal structure of phosphinothricin in the active site of glutamine synthetase illuminates the mechanism of enzymatic inhibition. Biochemistry 2001;40:1903–1912.
11. Liaw SH, Jun G, Eisenberg D. Interactions of nucleotides with fully unadenylylated glutamine synthetase from *Salmonella typhimurium*. Biochemistry 1994;33:11184–11188.
12. Krajewski WW, Collins R, Holmberg-Schiavone L, Jones TA, Karlberg T, Mowbray SL. Crystal structures of mammalian glutamine synthetases illustrate substrate-induced conformational changes and provide opportunities for drug and herbicide design. J Mol Biol 2008;375:217–228.
13. Llorca O, Betti M, Gonzalez JM, Valencia A, Marquez AJ, Valpuesta JM. The three-dimensional structure of an eukaryotic glutamine synthetase: functional implications of its oligomeric structure. J Struct Biol 2006;156:469–479.
14. Abergel C. Spectacular improvement of X-ray diffraction through fast desiccation of protein crystals. Acta Crystallogr D Biol Crystallogr 2004;60 (Part 8):1413–1416.
15. Leslie AGW. Recent changes to the MOSFLM package for processing film and image plate data. Joint CCP4 + ESF-EAMCB Newsletter on Protein Crystallography 1992, No. 26.
16. Evans PR. Data reduction. In: Proceedings of CCP4 Study Weekend, on Data Collection and Processing. Warrington: Daresbury Laboratory; 1993. pp 114–122.
17. Vagin A, Teplyakov A. MOLREP: an automated program for molecular replacement. J Appl Crystallogr 1997;30:1022–1025.
18. Murshudov GN, Vagin AA, Dodson EJ. Refinement of macromolecular structures by the maximum-likelihood method. Acta Crystallogr D Biol Crystallogr 1997;53 (Part 3):240–255.
19. Collaborative Computational Project Number 4. The CCP4 suite: programs for protein crystallography. Acta Crystallogr D Biol Crystallogr 1994;50 (Part 5):760–763.
20. Emsley P, Cowtan K. Coot: model-building tools for molecular graphics. Acta Crystallogr D Biol Crystallogr 2004;60 (Part 12, Part 1): 2126–2132.
21. Adams PD, Grosse-Kunstleve RW, Hung LW, Ioerger TR, McCoy AJ, Moriarty NW, Read RJ, Sacchettini JC, Sauter NK, Terwilliger TC. PHENIX: building new software for automated crystallographic structure determination. Acta Crystallogr D Biol Crystallogr 2002; 58 (Part 11):1948–1954.
22. Davis IW, Leaver-Fay A, Chen VB, Block JN, Kapral GJ, Wang X, Murray LW, Arendall WB, III, Snoeyink J, Richardson JS, Richardson DC. MolProbity: all-atom contacts and structure validation for proteins and nucleic acids. Nucleic Acids Res 2007;35 (Web Server issue):W375–W383.
23. Laskowski RA, Macarthur MW, Moss DS, Thornton JM. Procheck—a program to check the stereochemical quality of protein structures. J Appl Crystallogr 1993;26:283–291.
24. DeLano WL. The PyMOL Molecular Graphics System. DeLano Scientific LLC, San Carlos, CA, USA. Available at: http://www.pymol.org.
25. Corpet F. Multiple sequence alignment with hierarchical clustering. Nucleic Acids Res 1988;16:10881–10890.
26. Gouet P, Robert X, Courcelle E. ESPript/ENDscript: extracting and rendering sequence and 3D information from atomic structures of proteins. Nucleic Acids Res 2003;31:3320–3323.
27. Gill HS, Pfluegl GM, Eisenberg D. Multicopy crystallographic refinement of a relaxed glutamine synthetase from *Mycobacterium tuberculosis* highlights flexible loops in the enzymatic mechanism and its regulation. Biochemistry 2002;41:9863–9872.
28. Punekar NS, Vaidyanathan CS, Rao NA. Mechanisms of citric acid fermentation by *Aspergillus niger*. J Sci Ind Res 1984;43:267–287.
29. Schurke P, Freeman JC, Dabrowski MJ, Atkins WM. Metal-dependent self-assembly of protein tubes from *Escherichia coli* glutamine synthetase. Cu(2+) EPR studies of the ligation and stoichiometry of intermolecular metal binding sites. J Biol Chem 1999;274:27963–27968.
30. Yanchunas J Jr, Dabrowski MJ, Schurke P, Atkins WM. Supramolecular self-assembly of *Escherichia coli* glutamine synthetase: characterization of dodecamer stacking and high order association. Biochemistry 1994;33:14949–14956.